Chapter 12
Robotic Assistance for Cerebellar Reaching

David I. Grow, Amy J. Bastian, and Allison M. Okamura

Abstract Robotic instruments allow precise measurements and interventions to understand and treat human motor deficits. These same tools may be used to design model-based and patient-specific robotic assistance and rehabilitation paradigms. This approach could lead to an increased understanding of the brain and improved patient outcomes. We illustrate this paradigm with two studies in which generic and patient-specific models are used to provide reaching assistance with a robotic exoskeleton, the KINARM. These studies involve patients with cerebellar ataxia who make reaching movements that are irregularly curved, over- or undershoot targets, and are more variable than those of healthy people. Two assistive methods are explored. In the first, a patient-specific change in arm dynamics predicted to assist each patient is utilized. The results suggest this approach may improve the reaching of some cerebellar patients and not for others. The second method employs force channels, which improved reaching movements for all patients. However, neither method showed evidence of motor learning; i.e. there was no maintenance of improved movement after the assistive forces were removed.

Keywords Robotic assistance • Rehabilitation • Cerebellar ataxia

D.I. Grow (✉)
New Mexico Tech, 801 Leroy Pl., Socorro, NM 87801 USA
e-mail: dgrow@nmt.edu

A.J. Bastian
Kennedy Krieger Institute, Baltimore, MD, USA

Johns Hopkins University, Baltimore, MD, USA
e-mail: bastian@kennedykrieger.org

A.M. Okamura
Stanford University, Stanford CA, USA
e-mail: aokamura@stanford.edu

P. Artemiadis (ed.), *Neuro-Robotics: From Brain Machine Interfaces to Rehabilitation Robotics*, Trends in Augmentation of Human Performance 2,
DOI 10.1007/978-94-017-8932-5_12,

12.1 Introduction

Damage to the cerebellum results in ataxia, or a lack or coordination of volitional movements [1, 3, 13, 28, 33]. Point-to-point movements are often composed of an initial movement that under or overshoots the target (dysmetria), followed by a series of erroneous attempts at correction (intention tremor) [5]. In addition, cerebellar patients have difficulty adapting to changes in environment dynamics [8, 10, 19, 20, 24, 31]. People with ataxia almost always have normal strength. Cerebellar ataxia is difficult to treat; there are no medications that reliably reduce ataxia, making physical therapy and exercise the primary intervention. There is a need to understand the mechanisms of ataxia more completely to drive the development of rational physical therapy-based rehabilitation strategies. In this chapter, we present two methods for robotic assistance of cerebellar reaching (dynamic augmentation and force channels), and report their impact on the reaches of cerebellar patients, both during and after assistance.

12.1.1 Rehabilitation Robotics

The field of rehabilitation robotics involves the use of automatically controlled mechanisms to provide therapy and assistance to humans with disabilities [35]. As an alternative to human-only therapy, these devices permit: (1) consistent therapy without tiring; (2) precise measurements of behavior to quantify motor deficits and recovery; and (3) implementation of therapy paradigms not possible by a human therapist [20,30,31,35]. A wide variety of rehabilitation robots have been developed. One way to categorize these devices is by the way in which they physically connect to the user. One class are manipulandums – robots for upper-extremity therapy that connect to the user through a handle. An example of such a device that has been used extensively for clinical applications is the InMotion Arm Robot (originally called the MIT Manus). This device has undergone 20 years of development and has been used in research studies involving patients with stroke, cerebral palsy, and other neurological conditions [2, 12, 17].

Another class of rehabilitation robotic devices are exoskeletons, which couple to the user through multiple contact areas. An example of this type of device is the Lokomat by Hocoma, which is a lower-body exoskeleton and treadmill for gait therapy [36]. This device measures the user's gait and automatically augments the user's stride to provide individualized training.

Ideally, a rehabilitation robot would be able to provide many different forms of mechanical input, such as assisting, resisting, perturbing, and stretching, based on the subject's real-time response.

12.1.2 Robot-Assisted Rehabilitation Approaches

A robotic device can be programmed to apply forces that assist or resist the movements of the user. Assistive devices have been developed to extend the strength and dexterity of injured or diseased users as they walk, grasp objects, and perform other activities of daily living. Resistive devices, on the other hand, are used to retrain patients or minimize the undesired consequences of unintended motor activity.

Some common assisting methods include (1) passive motion, in which the robot moves the subject through a desired pattern, (2) active assistance, in which a subject-initiated movement is subsequently guided by the robot, (3) active constraint, or force channel, which allows subject motion only towards a target, and (4) mirror image, in which the less impaired arm motion is measured and used to guide motion of the more impaired arm [18].

Resistance to motion is achieved by a control law that increases forces opposing the subject's desired motion with speed and/or proximity to the target, such as a linear damping field [32]. Related to resistance training, feedback distortion can also be used in isometric and isotonic conditions to alter a subject's perception of therapeutic exercises [7]. Other work has exploited the after-effect of training forces (i.e. adaptation) that magnify original errors [11, 25]. With the capability to record motions and forces automatically, robotic systems can provide objective data to quantify how specific deficits change during training [35], as well as identify the mechanism of the deficit [20, 31].

12.1.3 Robot-Assisted Study of Neurological Impairments

Robots have also been used to study neurological impairments. Scheidt and Stoeckmann used a robot joystick to show that cerebral stroke subjects could use normal strategies based on error history to adapt movement, though not as efficiently as controls [27]. Patton et al. found that error-enhancing robot therapy improves reaching in stroke subjects more than control strategies that assist movement [25]. In contrast, subjects with cerebellar ataxia have been shown to be slowed or unable to adapt arm movements to novel forces, suggesting a deficient internal model of limb dynamics [20]. Interestingly, cerebellar subjects could correct on-line errors using feedback mechanisms, but could not adapt feedforward control mechanisms from trial to trial [31]. Subjects with Huntington's disease showed the reverse pattern, demonstrating that control mechanisms have distinct neural bases. Robotic devices can also be used to estimate human arm dynamics, as in [23].

12.2 Methods

The feasibility of uncovering cerebellar function and discovering a model of ataxia is bolstered by the availability of high-fidelity robotic exoskeletons. The field of robotics provides powerful tools for understanding the function of the cerebellum and other brain areas because it allows us to quantify and affect mechanical features of movement in a way not possible by direct human observation and manipulation. Here, we describe the robotic exoskeleton used in our experiments, our patient population, and two experiments (dynamic augmentation and force channels) that provide assistance to enhance cerebellar reaching.

12.2.1 KINARM Robot Motor and Controller Performance Characterization

In order to rigorously examine hypotheses about the function of the cerebellum, we require knowledge of actual limb dynamics and precise measurements of user reaching performance. Our studies used the KINARM robotic exoskeleton (Fig. 12.1, BKIN Technologies, Kingston, ON). The KINARM is an adjustable exoskeleton that permits bimanual shoulder and elbow rotation in the horizontal plane. This device has been used to acquire behavioral data during reaching [29]. In [15], a kinematic and dynamic model of the human arm and robot were developed and populated with parameter values obtained through direct measurement, system identification, and use of anthropometric tables. This provides a relationship between motor effort and movement.

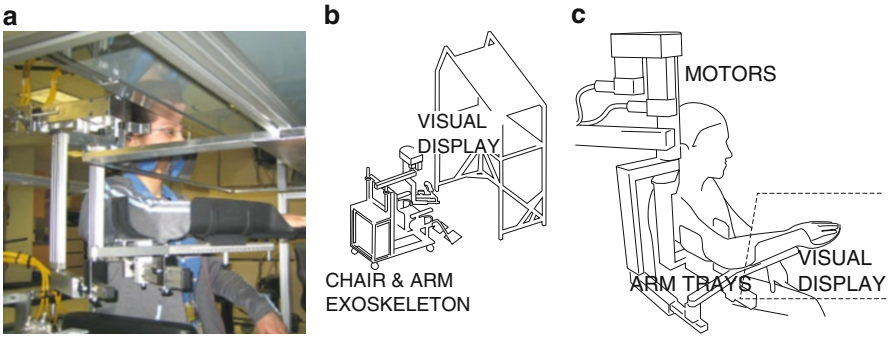

Fig. 12.1 The KINARM robot (**a**) used in this study has a two-degree-of-freedom planar exoskeleton for each arm (only right arm shown for clarity). The user sits in a chair (**b**) that is positioned so that the user's hand location and targets are visible on a horizontal display. The seat height, linkage lengths, and arm tray positions are adjusted for each user (**c**). Special care is taken to ensure that the rotational axes of the human shoulder and elbow are coincident with the corresponding joints of the KINARM. An advantage of the exoskeletal nature of the robot is that robot linkage and human arm kinematic parameters are determined simultaneously

The motors of the KINARM are controlled in an open-loop fashion. In order to understand the limits of the system's performance, we characterized the ability of motor controllers to follow a desired torque trajectory. Accurate calibration of motor gains is critical for accurate rendering of dynamic forces. For example, consider attempting to render arm inertia (mass matrix with non-negative scalars a, b, and c) while the shoulder and elbow motors have the non-unity gains ζ_1 and ζ_2. This torque scaling results in a corresponding scaling of the mass matrix:

$$\begin{bmatrix} \tau_{1_{act}} \\ \tau_{2_{act}} \end{bmatrix} = \begin{bmatrix} \zeta_1 a & \zeta_1 b \\ \zeta_2 b & \zeta_2 c \end{bmatrix} \begin{bmatrix} \ddot{\theta}_1 \\ \ddot{\theta}_2 \end{bmatrix}. \tag{12.1}$$

If $\zeta_1 \neq \zeta_2$, then the mass matrix is no longer symmetric – in essence, it no longer corresponds to any physically realistic inertia. In such a case, there would be no symmetry between the interaction torques of connected joints. A one-dimensional analog is a mass that feels heavier when moved forward than when moved backward.

12.2.1.1 Static Performance

To calibrate the static motor gains, the peak motor torque for each link was measured using a single-axis, hand-held digital force gauge (SHIMPO model FGV-50XY, Japan). The sensor was mounted tangentially to the robot link and coupled via a fitting that could not transmit substantial torque to the linkage. Thus, the reaction torque is the measured force multiplied by the moment arm. The torque trajectory was repeated four times at five different amplitudes for each motor.

12.2.1.2 Single-Joint Dynamic Performance

Next, the motor controller's performance while commanding velocity- or acceleration-dependent loads (viscosity/inertia) was characterized. The velocity, $\dot{\theta}$, and acceleration, $\ddot{\theta}$, signals are derived from a high-resolution encoder signal that is discretely differentiated. The process of differentiation scales the high-frequency (noise) content of a signal. To mitigate this effect, a running-average digital filter was used. This window must be larger to filter the acceleration signal compared to velocity.

The actual output torques were measured using an ATI Mini40 force/torque sensor (ATI Industrial Automation, Inc., Apex, NC; SI-20-1 calibration) mounted as before while the robot forearm was manipulated manually to follow a roughly sinusoidal position trajectory. The accuracy of the rendering was assessed by comparing the torques and kinematics using ordinary-least-squares regression [16]. If the desired coefficients for friction and inertia are f_b and I, the appropriate torque command τ_{com} is given by (12.2). Even when rendering only inertial or viscous

forces, the robot's inherent inertia and friction contribute to the force/acceleration relationship. As such, objective function (12.3) was used in all cases.

$$\tau_{com} = f_b\dot{\theta} + I\ddot{\theta} \tag{12.2}$$

$$\begin{bmatrix} \tau(t_1) \\ \tau(t_2) \\ \tau(t_3) \\ \vdots \end{bmatrix} = \begin{bmatrix} \theta(t_1) & \dot{\theta}(t_1) \\ \theta(t_2) & \dot{\theta}(t_2) \\ \theta(t_3) & \dot{\theta}(t_3) \\ \vdots & \vdots \end{bmatrix} \begin{bmatrix} f_b \\ I \end{bmatrix} \tag{12.3}$$

12.2.1.3 Multi-joint Dynamic Performance

In the first experiment, the KINARM is used to render the change in arm inertia predicted to help each patient. With active use of the robot, the mass matrix is composed of:

$$M_\theta = M_{human\ arm} + M_{robot\ linkage} + M_{rendered}. \tag{12.4}$$

Excessive noise or delay of the acceleration signal may result in poor rendering or instability. To reduce the noise and delay of the acceleration signal, two 2g 3-axis accelerometers (Crossbow Technology, Inc., San Jose, CA) were incorporated into each arm. Though substantially reduced, the residual noise presents an increasing challenge to system performance as the magnitude of the rendered inertia increases. Predicting whether some amount of rendered inertia will be achievable is a formidable problem because it depends on the robot setup and the patient's size, muscle tone, movement pattern, etc. As such, the rendered inertia must be gradually increased ($\epsilon \rightarrow 1$ in (12.5)) while the onset of noise or instability is monitored. It can be shown that any value of $0 < \epsilon < 1$ results in a qualitatively similar change to the total inertia ellipse – the eigenvectors, which determine the ellipse orientation, remain unchanged.

$$M_{rendered} = \epsilon \begin{bmatrix} \Delta a & \Delta b \\ \Delta b & \Delta c \end{bmatrix} \tag{12.5}$$

12.2.2 Human Subjects

Patients with damage to the cerebellum but no signs of sensory loss or extracerebellar damage were recruited. The severity of each patient's cerebellar impairment was determined using the International Cooperative Ataxia Rating Scale (ICARS) [34]. Table 12.1 lists cerebellar subjects ordered by the ICARS kinetic functions subscore, which assesses voluntary limb movements. Scores range from 0 (normal)

Table 12.1 Subject characteristics

Subject	Sex	Dominant hand	Age (years)	Height (m)	Weight (kg)	Diagnosis[a]	Limb score
Cerebellar 1	M	R	75	1.63	77	Stroke	13/52
Cerebellar 2	F	R	52	1.58	51	Stroke	15/52
Cerebellar 3	F	R	20	1.68	64	Trauma	18/52
Cerebellar 4	F	R	65	1.68	61	Sporadic	18/52
Cerebellar 5	M	L	37	1.78	123	SCA8	20/52
Cerebellar 6	M	R	56	1.80	90	SCA6,8	23/52
Cerebellar 7	M	L	57	1.70	96	ADCA	25/52
Cerebellar 8	F	R	69	1.70	68	Sporadic	23/52

[a]Spinocerebellar ataxia (SCA) diagnoses are described in [4]

to 52 (severe). Subject diagnosis is based on medical history, family history, and a neurological examination. The cause of ataxia may be abrupt damage to cerebellar tissue (stroke or trauma), genetic diseases (ADCA, SCA6, and SCA8), or unknown (sporadic) [4]. All subjects gave informed consent to the protocols approved by the Johns Hopkins Medical Institutions Review Board.

12.2.3 Methods of Robot Assistance

The anisotropic nature of arm inertia and other dynamic effects necessitate a non-trivial calculation of the muscle activity needed to reach rapidly in a given direction. It has been hypothesized that the cerebellum plays a key role in planning such movements and that damage to the cerebellum results in a degradation of the ability of the motor control system to plan these movements, accounting for the characteristic misdirection of observed arm movements [5, 6, 21, 22, 26]. The first assistive method explores this possibility in the attempt to derive an optimal, patient-specific assistance method. The second method applies a simple and generic method for assistance. As mentioned in Sect. 12.1, the cerebellum is thought to play a key role in accounting for (adapting to) changes in the dynamics. As such, subsequent to practicing with both of these assistive methods, additional null trials were incorporated into the experimental protocols to search for evidence of adaptation.

12.2.3.1 Assistance Method 1: Dynamics Augmentation

Phase 1: Identifying Optimal Augmentation

In [15], the KINARM robot was used to record the movements of cerebellar patients (Cerebellar 1–8, Table 12.1) performing a targeted reaching task. This task focused

on early movement because the role of the cerebellum is most observable during early movement. Subjects made center-out movements through 1 cm diameter targets at a 3 cm radius within a 350–650 ms window. Offline analysis of this data and the arm dynamic model were used to test various hypotheses proposed in the literature about the role of the cerebellum, all of which assume that the cerebellum functions as an internal model of limb dynamics for planning movements. It follows that damage to the cerebellum results in movements that do not properly account for arm dynamics. If this error is known, the potential exists for predicting reaching errors during early movement (before movement feedback is available).

During early movement, arm dynamics can be approximated as (12.6) [14, 15]. The parameters a, b, c, and d are all non-negative scalars, the first three relating to mass properties and the last relating to centripetal and Coriolis forces.

$$\begin{bmatrix} \tau_1 \\ \tau_2 \end{bmatrix} = \begin{bmatrix} a & b \\ b & c \end{bmatrix} \begin{bmatrix} \ddot{\theta}_1 \\ \ddot{\theta}_2 \end{bmatrix} + \begin{bmatrix} 0 & -2d & -d \\ d & 0 & 0 \end{bmatrix} \begin{bmatrix} \dot{\theta}_1^2 \\ \dot{\theta}_1 \dot{\theta}_2 \\ \dot{\theta}_2^2 \end{bmatrix} \tag{12.6}$$

Knowledge of each patient's arm dynamics allows inverse dynamic calculations to identify torque trajectories to each target. Because of the movements start from rest and are rapid, the magnitude of the acceleration greatly exceeds that of the velocity for the movements recorded. As such, the trajectories are insensitive to variations in d and so the computer simulations searched for a perturbation over the reduced set, $\{a, b, c\}$, that when used in forward dynamic simulations with the torque trajectories, optimally reduced reaching errors. Perturbations of this type are equivalent to reshaping and reorienting the arm inertia ellipse [9]. Though no change to arm dynamics was found that fully removed errors, patient-specific perturbations were found that resulted in a reduction in root-mean-squared directional reaching errors of 41 % averaged over 7 cerebellar patients.

Phase 2: Applying Prescribed Augmentation

A subset of these patients were available to return to perform a follow-up experiment to apply the dynamic augmentations predicted to most improve reaches. The KINARM robot was controlled to effectively reshape and/or increase or decrease the arm inertia. Three particular subjects were selected because distinct optimal perturbations were predicted and their ataxia severities spanned those of the group. These perturbations are summarized in Table 12.2 (columns 2–5). It follows that the opposite perturbation (i.e. $\{\Delta a, \Delta b, \Delta c\}$ vs. $\{-\Delta a, -\Delta b, -\Delta c\}$) would significantly hinder reaching performance, which could be a resistive approach to neurorehabilitation (see Sect. 12.1.2).

The task in this phase was nearly identical except that the center-out movements were to, not through, targets at a 10 cm, not 3 cm, radius. The more distant spacing of these targets compared to those in the Phase 1 task was chosen to permit

Table 12.2 A perturbation predicted to help patients was applied during a reaching task. The predicted optimal change in arm inertia, characterized by ellipse eccentricity, size, and orientation, for each subject is summarized along with the extent to which reaching performance is predicted to improve. The effect of applying the opposite perturbation (e.g. to reduce mass rather than add) was also explored with the goal of resisting rather than assisting movement. The full perturbation could not always be applied for stability reasons. During practice trials, conservatively safe values of ϵ (12.5) for each patient and for both the perturbation expected to help and hinder performance were determined and are also listed, ϵ_{help} and ϵ_{hinder}, respectively

Subject	Δ eccentricity (%)	Δ size (%)	Δ orientation (deg)	Predicted error reduction (%)	ϵ_{help}	ϵ_{hinder}
Cerebellar 1	−34	−61	1	37.5	0.8	0.8
Cerebellar 5	−14	−47	5	62.5	1.0	0.75
Cerebellar 6	−39	−99	2	62.9	0.3	0.3

investigation of the method's effect on movement both before and after peripheral feedback can be used. Another subtle difference compared to the preliminary studies is that four, rather than eight, targets were used to obtain a greater number of reaches to each target.

At the beginning of each trial, the subject moved to a center position (shoulder at 35°, elbow at 90°). After a slight delay, one of four targets appeared randomly, to which subjects were directed to move within a 200–550 ms time window. Trials were divided into five blocks (Fig. 12.2). Movement duration feedback was given to the subjects in the form of color coding: the target turned blue if reached late, red if early, or green if on time. At the end of each trial, the actual hand path taken was shown to subjects. All trials were analyzed, whether or not the timing criteria were met.

To ensure that the robot would remain stable throughout the experiment, the magnitude of the inertia perturbation, ϵ, was gradually increased towards the desired magnitude while patients practiced the target reaching movements until the onset of instability was detected. This detection was done using digital scopes that report the joint accelerations and motor commands where the onset of instability was evident well before it was perceptible to the subject, resulting in a conservative limit. For the patients tested, the level of perturbation rendered varied from $\epsilon = 30$–$100\,\%$ (12.5). Force levels and dynamic perturbations are given in Table 12.2, columns 6 and 7.

Reaching performance was measured using lateral deviation Δ_{err} of the finger at 150 ms (12.7), where the finger location and target vectors are $\mathbf{p}$ and $\mathbf{t}$, respectively (Fig. 12.3). It is computed as:

$$\Delta_{err} = \left\| \mathbf{p}(150) - \frac{\mathbf{p}(150) \cdot \mathbf{t}}{\|\mathbf{t}\|^2} \mathbf{t} \right\|. \tag{12.7}$$

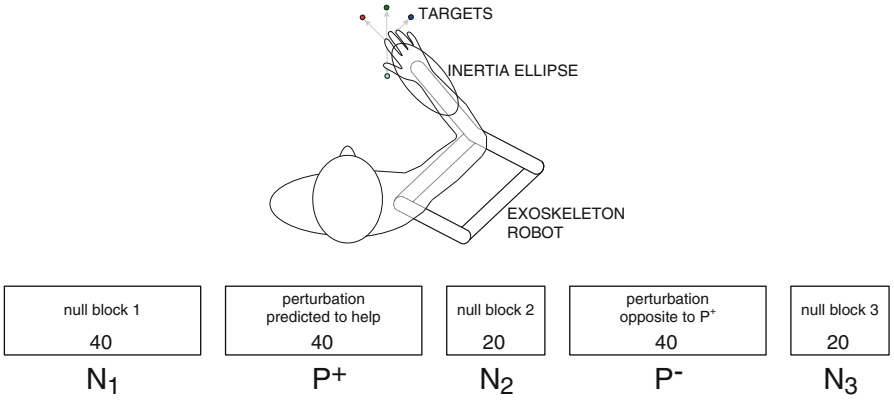

Fig. 12.2 Horizontal reaching task with augmented arm inertia. During the null blocks $\{N_1, N_2, N_3\}$, the robot is passive as the patient moves to one of four targets, the blocks containing 40, 20, and 20 trials, respectively. During the first perturbation block P^+, the robot augments arm inertia in a manner predicted to help as the subject makes a total of 40 reaches to 4 targets. The second perturbation block P^- is identical except the robot augments arm inertia with the opposite sign

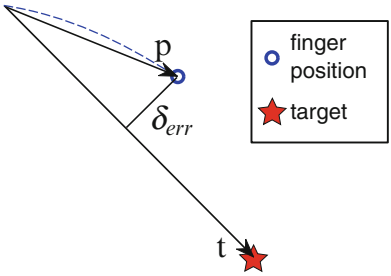

Fig. 12.3 Depiction of error metric: lateral deviation of the finger position from the target path (12.7)

12.2.3.2 Assistance Method 2: Force Channel Rendering

This potential reaching assistance method applies force channels designed to improve reaching performance by enforcing the coordination needed to follow a straight path. Furthermore, these channels are used in an attempt to elicit use-dependent learning, or improvements in both the straightness of the path (lateral error) and the ability to stop at the target (overshoot error) subsequent to channel reaching.

Six cerebellar patients performed this experiment (Cerebellar 2 and 4–8 in Table 12.1). Because it has been reported that use-dependent learning is stronger when the non-dominant arm is trained, that arm was tested whenever possible. The one exception was the case of Cerebellar 6, whose non-dominant arm had a reduced range of motion. Also, Cerebellar 5 was available to have both arms tested.

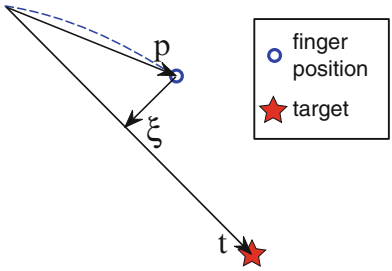

Fig. 12.4 The KINARM robot is used to render force channels that assist a user in moving in a straight direction to targets. The force generated is perpendicular to and scales linearly with deviation from the desired path (12.8)

Force channels were rendered by the KINARM to provide a simple form of assistance during reaching. These channels act as virtual walls to constrain movement by applying a forces perpendicular to the desired direction of movement. The forces are smooth and allow the subject to maintain complete control over the speed of movement. Figure 12.4 illustrates the relationship between finger position, target location, and the spring-like force generated. Given the positions of the finger, $\mathbf{p}$, and target, $\mathbf{t}$, the channel force with stiffness k_c in Cartesian space is given by:

$$\begin{aligned} \boldsymbol{\xi} &= \frac{\mathbf{p} \cdot \mathbf{t}}{\|\mathbf{t}\|^2} \mathbf{t} - \mathbf{p} \\ \mathbf{f} &= k_c \, \boldsymbol{\xi} . \end{aligned} \tag{12.8}$$

As before, subjects were directed to make point-to-point movements. At the beginning of each trial, the subject moved to a center position (shoulder at 35°, elbow at 90°). After a slight delay, a target appeared in one of four radial targets, again 10 cm away and to be reached within a 200–550 ms window with as straight a movement as possible. Using the same color-coding as in the augmentation experiment and by showing a trace of the actual movement path after each reach, subjects were given feedback after each reach about timing and movement accuracy, respectively. Spatial feedback was given after each reach. All trials were analyzed, whether or not the timing criteria were met. Two experimental protocols were used to address questions about reaching direction, prolonged training, and generalization of learning. The organization of each protocol and the differences between them are given in Fig. 12.5.

Reaching performance during null and force-channel blocks was measured using four metrics:

M_1: Path length is computed by integrating changes in finger position over the duration of movement:

$$\text{path}_{err} = \sum_n \|\mathbf{p}(n) - \mathbf{p}(n-1)\| . \tag{12.9}$$

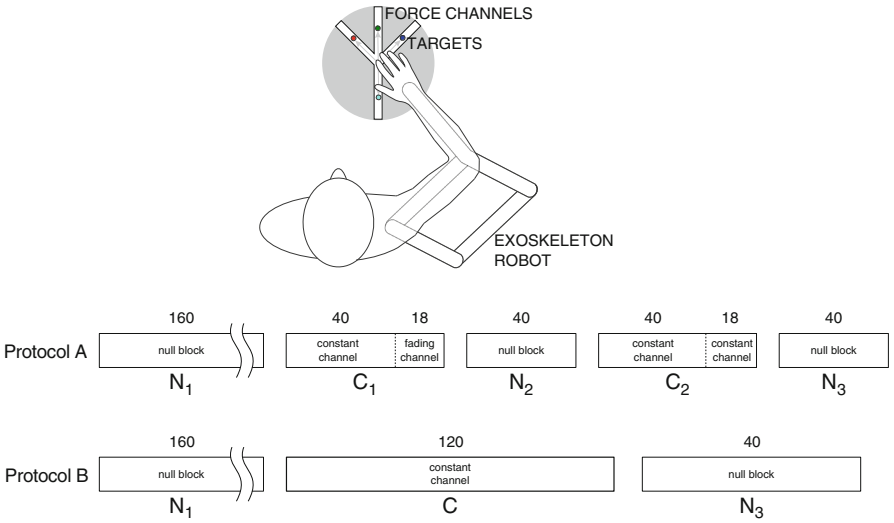

Fig. 12.5 Horizontal reaching task with force channels. One of four targets with 1 cm diameter appear in pseudo-random order at 10 cm from start position. In Protocol A there are seven blocks with $\{160, 58, 40, 58, 40\}$ trials each. Three null (robot passive) blocks $\{N_1, N_2, N_3\}$ are separated by force channel (robot active) blocks. During the first channel block C_1, the robot generates a force channel and the subject makes 40 reaches *only to the 12:00 target* followed by 18 more reaches while the channel is gradually removed. The second channel block C_2 is identical except that the force channel remains at full strength for 58 reaches. During these channel blocks assistance is only provided for the 12:00 direction. By looking at other directions during null trial blocks, evidence of learning generalization is sought. In Protocol B there are three blocks with $\{160, 120, 80\}$ trials each. Two null blocks are separated by a channel block where force channels are rendered to *each* of the four targets. Another difference from Protocol A is the extended length of the training blocks to investigate whether learning would arise from prolonged training

M_2: Maximum lateral deviation throughout the trial is computed by:

$$\Delta_{err} = \arg\max_{n} \left\| \mathbf{p}(n) - \frac{\mathbf{p}(n) \cdot \mathbf{t}}{|\,\mathbf{t}\,|^2}\,\mathbf{t} \right\|. \tag{12.10}$$

M_3: Lateral deviation at 150 ms is computed as described previously (12.7).

M_4: Overshoot is computed by finding the finger position at the first velocity zero crossing, $\mathbf{p}(n_0)$, and computing the displacement of this point from the target (Fig. 12.6):

$$\eta_{err} = \left\| \mathbf{t} - \arg\max_{n \le n_0} \|\mathbf{p}(n)\| \right\|. \tag{12.11}$$

Differences in performance between null and channel trial blocks were checked for statistical significance using a Kruskal-Wallis non-parametric test. This test

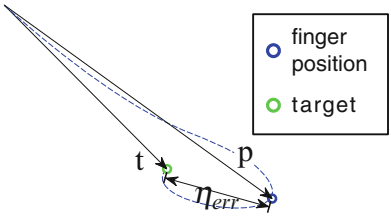

Fig. 12.6 Depiction of the overshoot error metric: the distance between the target and the point of maximum excursion (12.11). We only consider the portion of movement until the first zero-crossing

is well suited to these data because the variability of the error metrics tends to change significantly during channel trials, violating the sphericity assumption of the Analysis of Variance (ANOVA).

12.3 Results

12.3.1 Motor and Controller Performance Characterization

12.3.1.1 Static Performance

For each commanded torque amplitude and for each motor, four torque measurements were taken and averaged. Linear regression of this data yields a calibration coefficient for each motor (Fig. 12.7). Each slope is inverted to determine the appropriate gain to apply to the motor torque command (e.g. a slope of 0.95 prescribes a 1.05 gain). Fortunately, the motor gains are all within 10 % of unity. This degree of miscalibration does appear to vary in time, but can be accounted for by scaling commanded torques accordingly in software. The appropriate adjustments in motor gains were determined from the open-loop, near-static conditions shown in Fig. 12.7 by taking the inverse of the slopes.

12.3.1.2 Single-Joint Dynamic Performance

Even after calibration, the open-loop torque controller may not be linear under non-static conditions. From Fig. 12.8, it is clear that the open-loop performance is inaccurate if the frequency content exceeds 7 Hz.

In the case of a perfect sinusoidal position trajectory, the velocity and acceleration signals are scaled versions of the position with phase shifts of 90° and 180°, respectively. Because inertial forces are rendered by simply scaling the acceleration signal, the same delay persists. Thus, this delay makes rendered inertial forces behave increasingly like viscosity. The overall delay in the system is appreciable and in fact, when attempting to render inertia, a least-squares regression of the resulting forces are identifies increases in both inertia and damping. A smaller filter (and thus

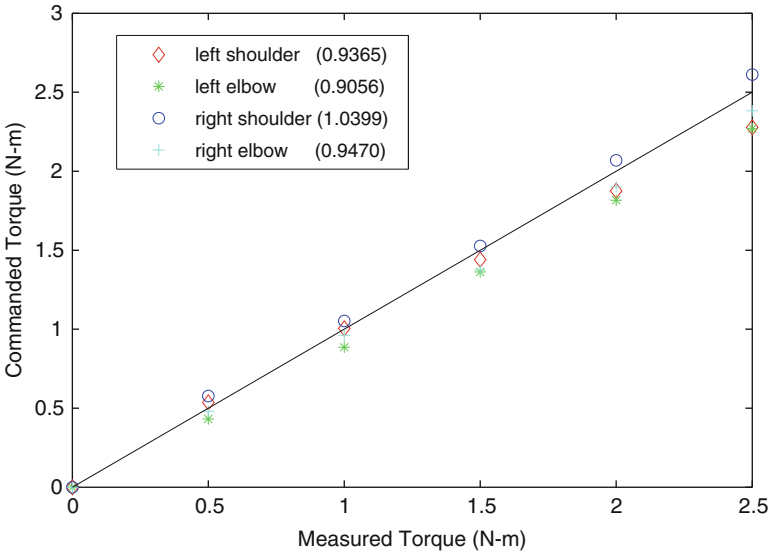

Fig. 12.7 Measured vs. commanded torque trajectories were recorded as sinusoidal torque trajectories were commanded to each of the four motors (From this data, calibration factors were determined)

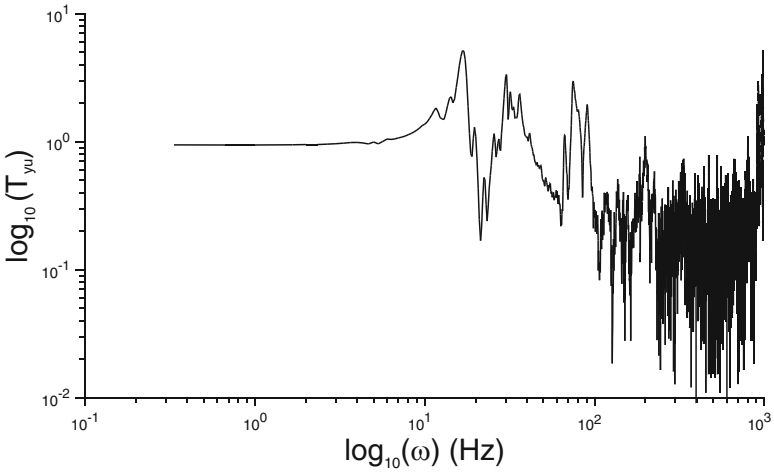

Fig. 12.8 The ratio of angular acceleration to commanded torque T_{yu} at the elbow joint is plotted as a function of angular frequency. Note the near unity gain for low frequencies and degraded (non-unity gain) at higher frequencies

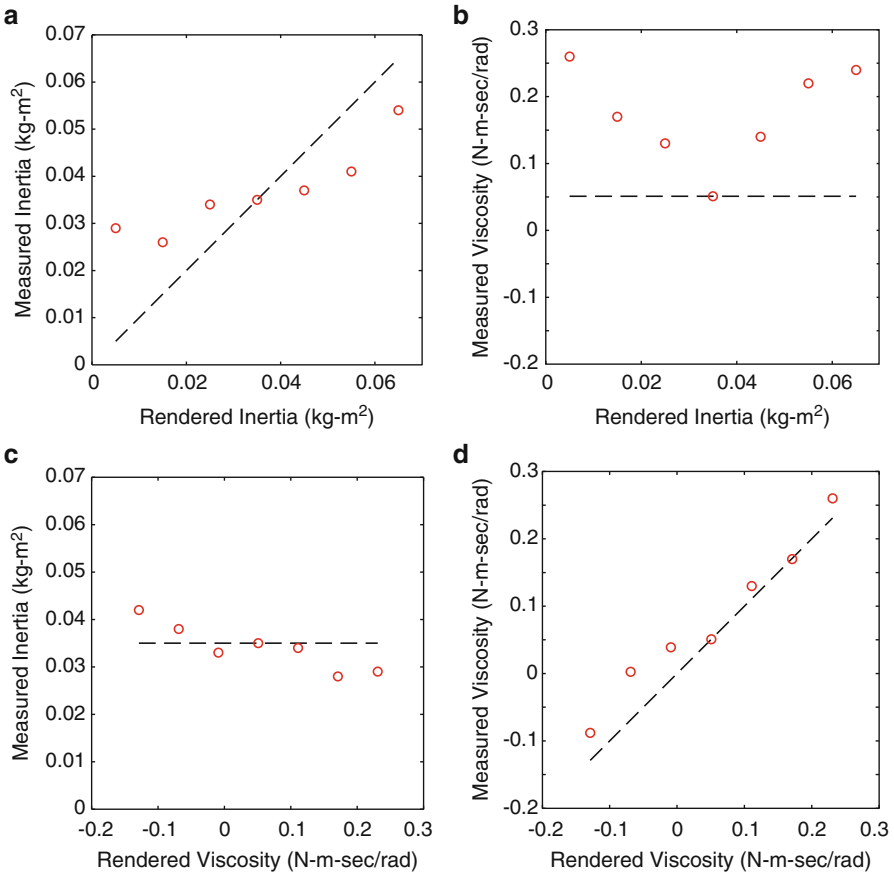

Fig. 12.9 The ability of the robot to render viscous and inertial torques is investigated. In (**a**), virtual inertia is added by the robot increasing and decreasing the base inertia in steps of 0.01 kg-m^2. In (**b**), an undesired effect on the forearm viscosity while rendering inertia is shown. In (**c**), an undesired effect on the forearm inertia while rendering viscosity is shown. In (**d**), virtual viscosity is added by the robot increasing and decreasing the base viscosity in steps of 0.03 N-m-s/rad

smaller delay) applied to the velocity signal results in forces that are identified as being nearly pure viscosity of the target magnitude, the identified inertia remaining relatively constant across rendered viscosity magnitudes (Fig. 12.9). In Fig. 12.10, the raw data used for regression are shown. The individual data points in each of the sub-figures are of no particular significance – they are specific to the manual perturbations applied. However, the covariance of the points is significant. If the dynamics consist of inertia only, an angular acceleration vs. torque point cloud will have a nonzero slope that corresponds to the inertia and the angular velocity vs. torque point cloud will have a zero slope. The opposite is true if the dynamics consist only of viscosity. If both inertia and viscosity are present, both clouds will have a

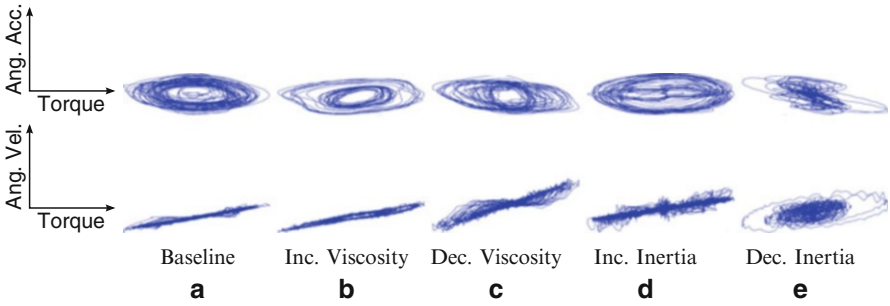

Fig. 12.10 The elbow joint of the robot is manipulated manually while various dynamic effects are rendered. The collected data are used for dynamic parameter identification. Representative data is shown to conceptually illustrate the process of regression: (**a**) baseline condition (robot passive), robot adds (**b**) or subtracts (**c**) viscosity, and robot adds (**d**) or subtracts (**e**) inertia

Table 12.3 Inertia values about shoulder and elbow joints at baseline and as measured during the rendering of reduced inertia compared to that desired change in inertia

	Joint	Baseline (kg-m^2)	Desired change (kg-m^2)	Measured change (kg-m^2)
Left	Shoulder	0.1313	−0.0500	−0.0377
	Elbow	0.0387	−0.0150	−0.0068
Right	Shoulder	0.1313	−0.0520	−0.0377
	Elbow	0.0387	−0.0142	−0.0068

nonzero slope. This procedure was duplicated with the other arm, and then at the shoulder of each arm. The results of rendering reduced inertia at each of the four joints are summarized in Table 12.3.

12.3.1.3 Multi-joint Dynamic Performance

As in the one-dimensional case, inertia rendering fidelity is affected by filter delay. The measured versus commanded torques while rendering various simple dynamic perturbations are shown in Fig. 12.11.

12.3.2 Assistance Method 1: Dynamics Augmentation Results

Data collected from the patients are included in several figures that follow. The hand paths and errors are shown for each of the five trial blocks. Because reach direction is the movement feature of interest, lateral deviations at 150 ms are shown both as block averages and for individual reaches. The individual data for Cerebellar 5, who has moderate ataxia, is shown in Fig. 12.12. It is evident that the patient benefited from the prescribed perturbation in effect (reduced lateral deviations). Similarly, the

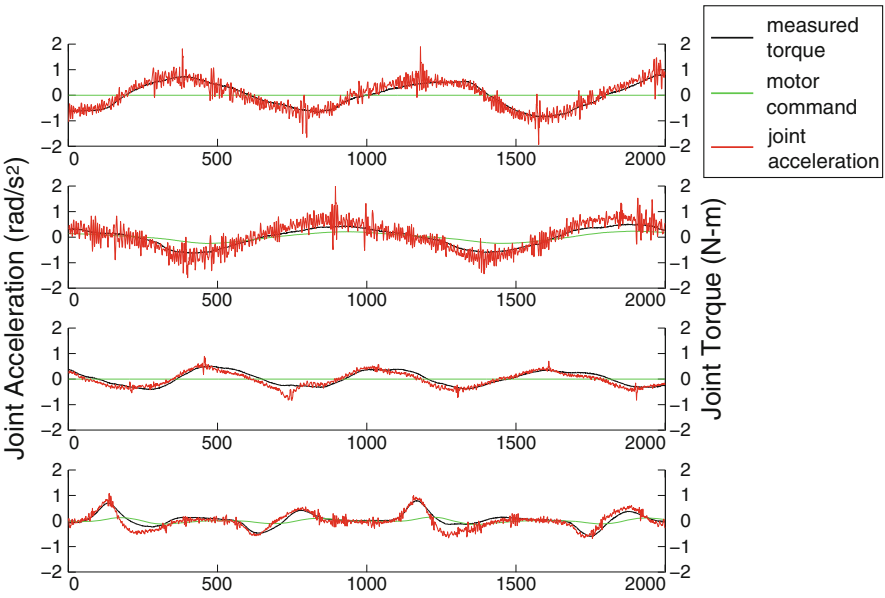

Fig. 12.11 Measured acceleration vs. commanded torque trajectories. During passive perturbations (row 1, shoulder and row 3, elbow), the acceleration and the torque measured via a force/torque sensor are linearly dependent. During active perturbations (row 2, shoulder and row 4, elbow), the motor command can be seen to lag the acceleration. This delay is more profound for rapid (row 4) movements

opposite perturbation resulted in degraded movement performance. The results for Cerebellar 1 (mild ataxia) and 6 (severe ataxia) are not as consistent across direction, but show a similar trend [15].

12.3.3 Assistance Method 2: Force Channel Results

The data were analyzed according to each of the four error metrics ($M_1 - M_4$) and differences in performance were checked for statistical significance. Representative recorded movements and performance measurements for subjects tested under Protocol A and Protocol B are included in Figs. 12.13 and 12.14, respectively. Summaries of the results including statistical test outcomes are given in Figs. 12.15 and 12.16.

During channel blocks, performance was significantly improved (Table 12.4). Error metrics M_2 and M_3 decreased in all four directions in both Protocols A and B. Significant improvement in overshoot error was observed in the 12:00 and 6:00 directions under Protocol A. We also found a significant improvement in path length for the 12:00 target under Protocol A (Table 12.4).

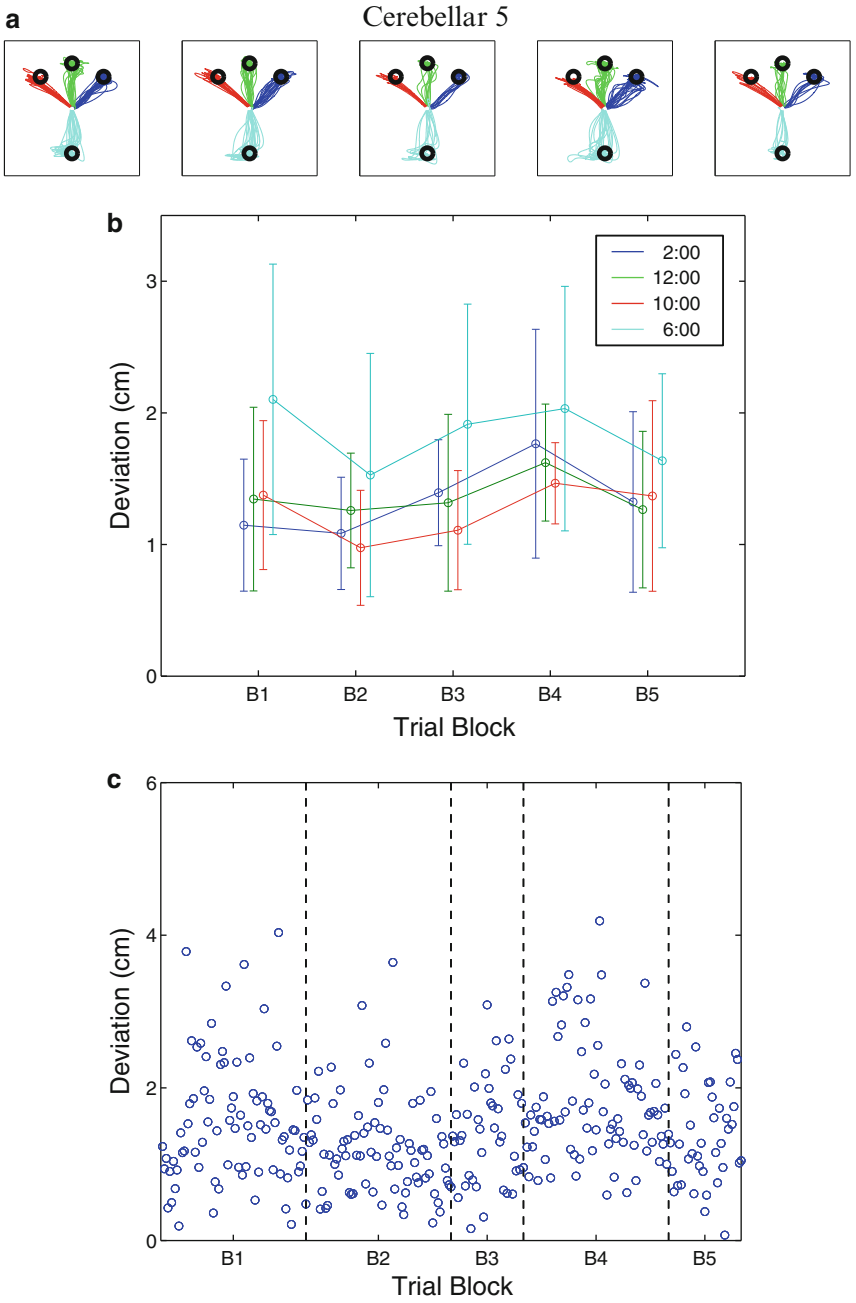

Fig. 12.12 Cerebellar Subject 5 makes targeted reaching movements to four targets while the robot provides Assistance Method 1. The task is divided into five blocks. The first, third, and fifth are null blocks where the robot is passive. During the second block, the robot affects arm dynamics in a manner predicted to help. During the fourth block, the opposite change in dynamics is made, which we expect to hinder performance. Hand paths and errors are color coded by direction

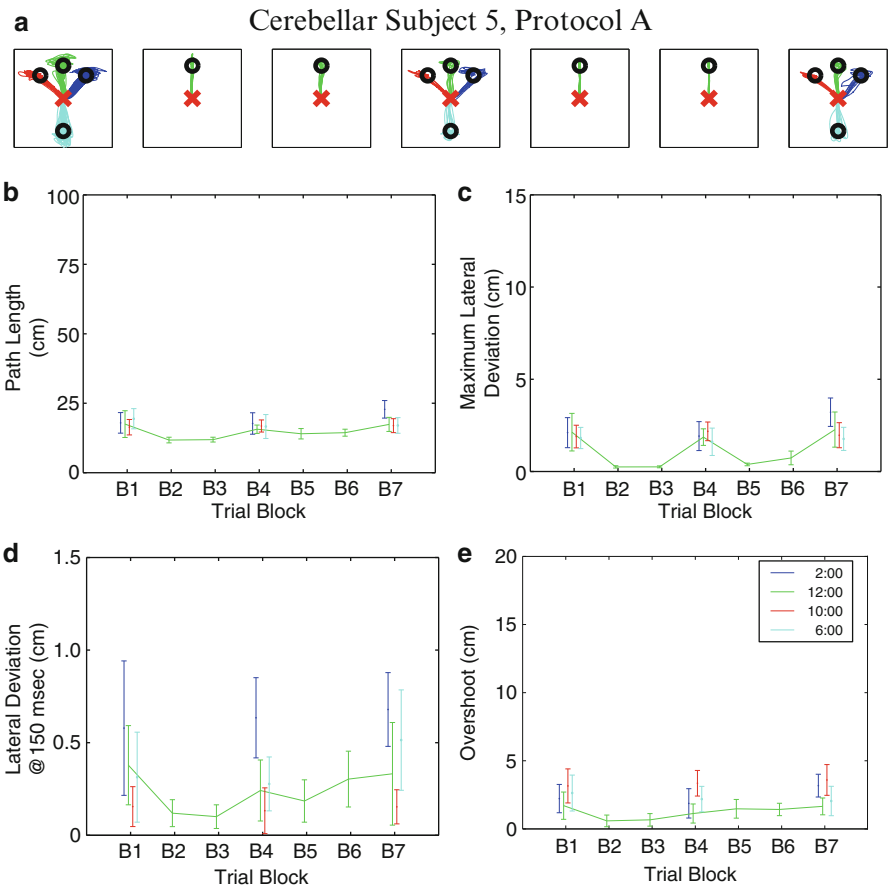

Fig. 12.13 Cerebellar Subject 5 makes targeted reaching movements to four targets while the robot provides assistance Method 2, Protocol A. The task is divided into seven blocks. The first, fourth, and seventh are null blocks where the robot is passive and subjects move to each of the four targets. During the second, fifth, and sixth blocks, the robot renders a force channel that assists the patient in moving in a straight path to the 12:00 target only. During the third block, the force channel begins at full strength and is reduced linearly to zero strength over the course of the block. Reaching performance is measured using the error metrics described in Sect. 12.2.3.2. Hand paths and errors are color coded by direction

Learning would be evidenced by residual improvements in performance after the removal of force channels. However, whether the force channel was removed gradually (Protocol A, $B_3 \rightarrow B_4$) or abruptly (Protocol A, $B_6 \rightarrow B_7$ or Protocol B, $B_2 \rightarrow B_3$) no learning was identified (Table 12.5).

We also looked for generalization by comparing performance in the non-trained directions (2:00, 10:00, and 6:00) after a block of channel trials. We found no evidence of generalization according to any of the error metrics (Table 12.6).

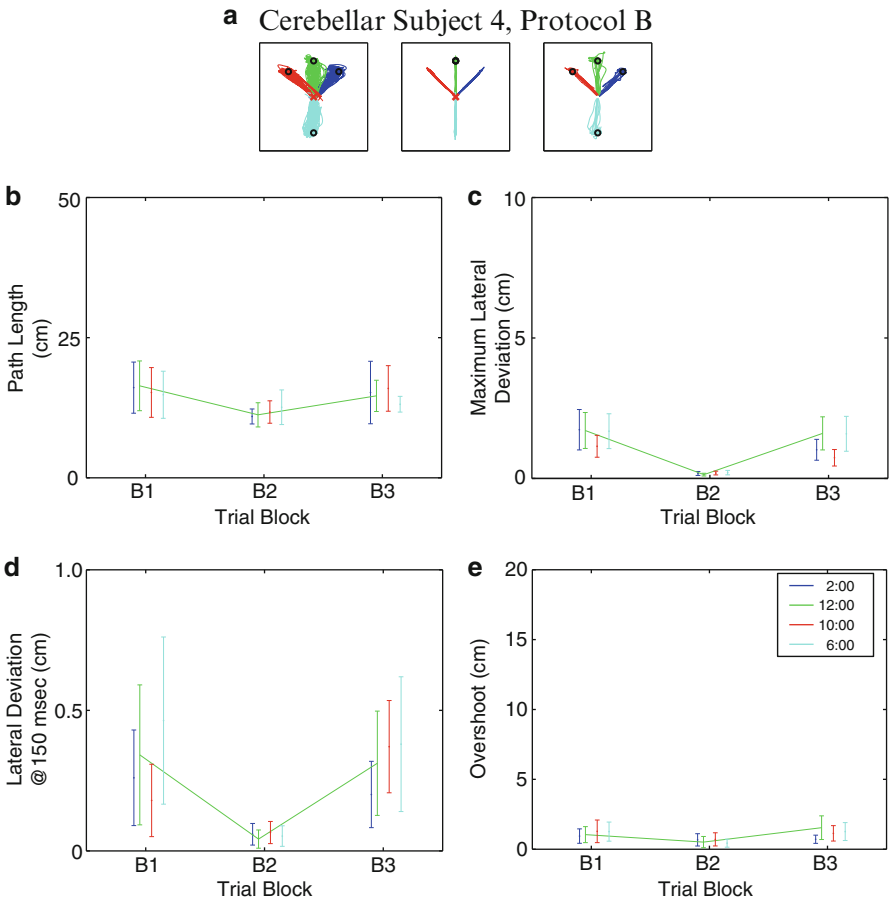

Fig. 12.14 Cerebellar Subject 4 makes targeted reaching movements to four targets while the robot provides assistance Method 2, Protocol B. The task is divided into three blocks. The first and third are null blocks where the robot is passive. During the second block, the robot renders a force channel that assists the patient in moving in a straight path to the target. Reaching performance is measured using the error metrics described in Sect. 12.2.3.2. Hand paths and errors are color coded by direction

12.4 Discussion

12.4.1 Motor and Controller Performance Characterization

The fidelity of dynamic forces rendered by the KINARM was characterized in detail. For this particular robot, the ability to render inertia was somewhat limited, although the performance is linear up to approximately 7 Hz. Performance was

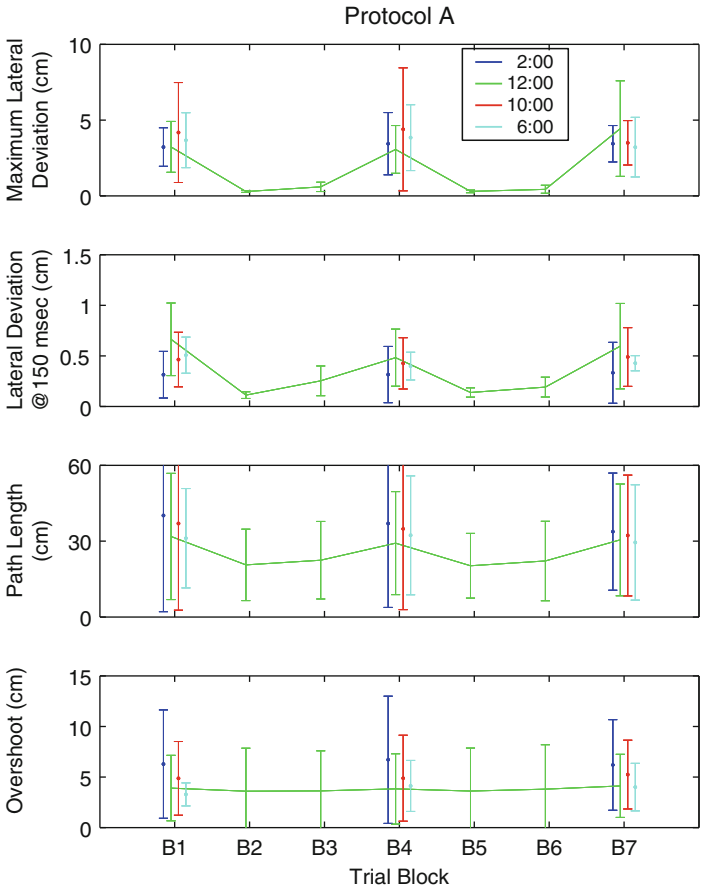

Fig. 12.15 Summary of force channel results under assistance Method 2, Protocol A. Three patient data sets are averaged. Four metrics are used to measure performance – maximum lateral deviation from the straight path (first row), lateral deviation at 150 ms from the straight path (second row), path length (third row), and overshoot (fourth row). The only direction in which statistically significant changes in performance were observed is the 12:00 direction. Hand paths and errors are color coded by direction

increased with the addition of accelerometers and tuned digital filters. We designed controllers and instrumentation, and validated the ability of the robot to render desired acceleration-dependent forces. The quality of the dynamic forces rendered was sufficient, and, when necessary, the magnitude of dynamics perturbations were reduced in scale to ensure patient safety and controller stability. Robot friction parameters were identified, but were found to contribute insignificantly to the overall dynamics.

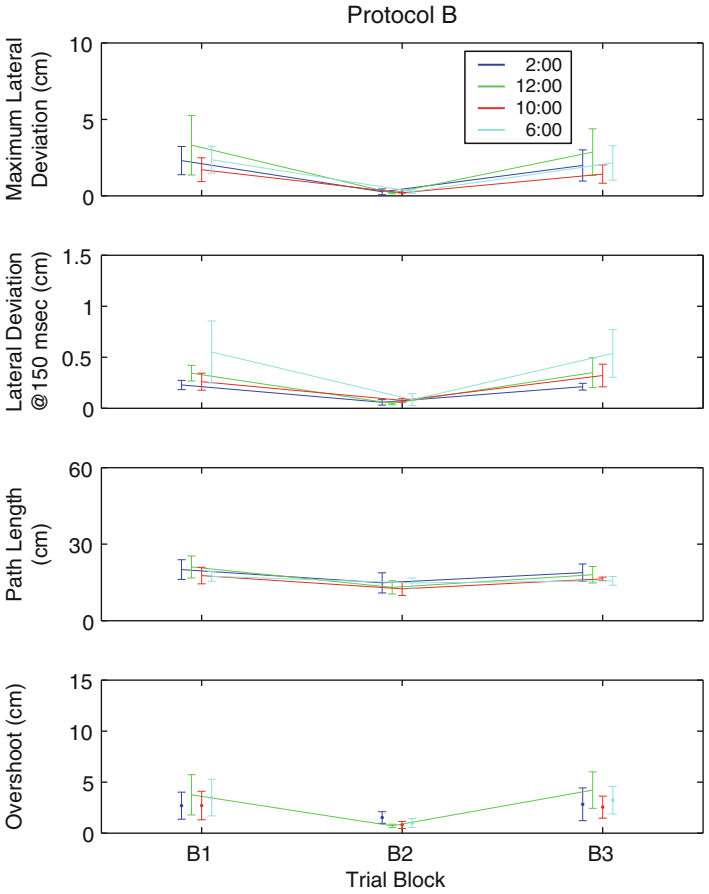

Fig. 12.16 Summary of force channel results under assistance Method 2, Protocol B. Four patient data sets are averaged. Four metrics are used to measure performance – maximum lateral deviation from the straight path (first row), lateral deviation at 150 ms from the straight path (second row), path length (third row), and overshoot (fourth row). Hand paths and errors are color coded by direction

12.4.2 Assistance Method 1: Dynamics Augmentation

Patient-specific changes in arm dynamics predicted to assist in making straight reaching movements were tested in this study. The results suggest this dynamics augmentation approach may improve the reaching of some cerebellar patients and not others. There was no evidence of motor learning.

The mildly impaired patient, Cerebellar 1, demonstrated near-control-like reaching performance in all five blocks. Even during B_2 and B_4 when substantial perturbations were applied, the patient performed nearly as well as control subjects.

Table 12.4 Nonparametric test p-values are listed for various metrics and reaching directions (p-values less than 0.05 are printed in boldface). In this test, errors during the null blocks are compared to errors during channel blocks ($\{B_1, B_4, B_7\}$ vs. $\{B_2, B_3, B_5, B_6\}$ under Protocol A and $\{B_1, B_3\}$ vs. B_2 under Protocol B). Significant improvements in performance were observed as patients reached in force channels

Protocol A $\{B_1, B_4, B_7\}$ vs. $\{B_2, B_3, B_5, B_6\}$				
Direction	M_1 (path length)	M_2 (max lateral dev)	M_3 (dev at 150 ms)	M_4 overshoot
12:00	0.2752	**0.0495**	**0.0495**	0.5127
Protocol B $\{B_1, B_3\}$ vs. B_2				
Direction	M_1	M_2	M_3	M_4
2:00	0.2482	**0.0209**	**0.0209**	0.3865
12:00	**0.0433**	**0.0209**	**0.0209**	**0.0209**
10:00	0.0833	**0.0209**	**0.0209**	0.1489
6:00	0.1489	**0.0209**	**0.0209**	**0.0433**

Table 12.5 Nonparametric test p-values are listed for various metrics and reaching directions. In this test, errors during the null blocks are compared to each other ($\{B_1, B_4, B_7\}$ under Protocol A and $\{B_1, B_3\}$ under Protocol B). No evidence of use-dependent learning was observed

Protocol A B_1 vs. B_4 vs. B_7				
Direction	M_1 (path length)	M_2 (max lateral dev)	M_3 (dev at 150 ms)	M_4 overshoot
12:00	0.9565	0.7326	0.7326	0.9565
Protocol B B_1 vs. B_3				
Direction	M_1	M_2	M_3	M_4
2:00	0.3865	0.3865	0.3865	0.7728
12:00	0.1489	0.3865	1	0.7728
10:00	1	0.5637	0.5637	0.7728
6:00	0.1489	0.7728	1	1

Table 12.6 Nonparametric test p-values for various metrics and reaching directions. In this test, errors to the non-trained reaching directions during the null blocks $\{B_1, B_4, B_7\}$ under Protocol A are compared to each other. Generalization of use-dependent learning was not observed

Protocol A B_1 vs. B_4 vs. B_7				
Direction	M_1 (path length)	M_2 (max lateral dev)	M_3 (dev at 150 ms)	M_4 overshoot
2:00	0.5866	0.8752	0.9565	0.9565
10:00	0.7326	0.9565	0.4298	0.8371
6:00	0.7326	0.9565	0.6703	0.9565

This indicates that some capacity for motor adaptation remains for this subject and a potentially substantial subset of the patient population. This contradicts one of our key assumptions made during the computer simulations used to find the optimal perturbation: in accordance with the many studies which have shown impaired motor adaptation among cerebellar patients, the simulations assumed cerebellar patients repeat the same pattern of muscle activity during early movement. Violations of this assumption would result in a perturbation that will not remain optimal over time. Real-time optimization of this perturbation might result in further improvement for patients capable of motor adaptation.

For the moderately impaired patient, Cerebellar 5, performance improved with the P^+ perturbation and degraded with the P^- perturbation, as predicted (lateral deviation decreased 16 % with P^+ and increased 19 % with P^-). These results suggest that this model-based approach may be useful, at least for some subset of patients. However, more experiments must be done to better understand the efficacy of this approach.

With the severely impaired patient, Cerebellar 6, no clear pattern was observed. Though this method can only address the repeated misdirection, or bias, in reaching, ataxia results in both misdirected and highly variable movements. This subject's movements were particularly variable and it is possible that the robot's effect on reaching dynamics does not exceed some critical, noise-dependent threshold. We also suspect that this patient's shoulder injury may obscure these results.

12.4.3 Assistance Method 2: Force Channel

In this second study, the robot was used to render force channels to constrain arm movements during reaching. This study also explored how the ordering of null (robot passive) and channel (robot active) trial blocks affected motor learning. The force channels resulted in significant improvements in reaching performance in the directions both parallel and orthogonal to the force channel. There was no evidence that reaching practice in these channels results in improved reaching performance after the channels were removed.

It may be seen as a trivial observation that force channels had a significant effect of decreasing lateral deviation – this is precisely the function of the channel. However, the presence of force channels also had an effect on overshoot in the 12:00 and 6:00 directions. In other words, patients not only made straighter movements, but in two of the four directions, demonstrated improvement in the direction orthogonal to the channels. This is analogous to the observation that cerebellar subjects are less impaired when making single-jointed movements [5], in that the channels simplify motor control requirements.

Our failure to observe learning is consistent with many other cerebellar studies. Indeed, a common theme in cerebellar studies is that error-based or use-dependent learning mechanisms are difficult to elicit. We found that the gradual removal of the force channel did not produce a measured effect.

12.5 Conclusions

The first assistance method explored here utilizes the KINARM exoskeleton to apply the optimal augmentation in dynamics for specific cerebellar patients. In essence, the goal is to "add back in" the aspects of limb control that have been lost for each cerebellar subject. It appears that this targeted, assistive approach may work for some patients. This work could be extended by improving the fidelity and range of dynamic perturbations that the robot can stably render. This could possibly increase the number of patients and the degree to which each is assisted by this method.

This approach could lead to a "soft" rehabilitation strategy in which wearable devices are used to change effective limb dynamics in a manner that exactly counters the original movement deficit, thus providing patient-specific, unconstrained robotic assistance or training for movement control. An approach like this would be especially useful as correcting faulty cerebellar patient movements through motor learning has proven elusive [10, 19, 20, 31]. These results inspire the design of new assistance strategies for patients with cerebellar damage using patient-specific augmentations to arm dynamics. Critically, such an approach could improve reaching performance without knowing the patient's intended direction of movement a priori.

The motor behavior does, at least for some cerebellar patients, change in the presence of an altered dynamic environment. One approach to account for this is to apply a prescribed perturbation, measure performance, recalculate the optimal perturbation, and iterate. Faster simulation and optimization may enable this approach in future work.

The second assistive method uses force channels and explores task designs that might elicit use-dependent learning with cerebellar patients. The KINARM is able to stably render stiff force channels that significantly improve reaching performance. However, reaching performance returned to baseline after the channels were removed. We also were not able to detect generalization of learning – practice in a force channel had no effect of subsequent reaching behavior in other directions.

The design of effective training protocols for cerebellar subjects is certainly a challenge given the reality of their loss of brain function. However, much redundancy does exist in the human motor control system and other learning mechanisms might be engaged through clever task design. The importance of informed task design is critical given the logistical difficulty in recruiting patients with a very specific condition. In parallel to these efforts, wearable devices could be designed to implement assistive strategies to improve patients' quality of life by assisting them with activities of daily living.

These studies demonstrate the use of robotic instruments for precise measurements and interventions to understand and treat human motor deficits. In particular, the capacity to affect the dynamics of the human arm in an arbitrary manner allowed for a direct test of a popular hypothesis about cerebellar function and is something that could not be practically achieved with any other instrument. The approach of designing model-based and patient-specific robotic assistance and rehabilitation paradigms could lead to an increased understanding of the brain and improved patient outcomes.

References

1. Adams R, Victor M (1993) The cerebellum. Principles of neurology. McGraw-Hill, OH
2. Aisen M, Krebs H, Hogan N, McDowell F, Volpe B (1997) The effect of robot-assisted therapy and rehabilitative training on motor recovery following stroke. Arch Neurol 54(4):443–446
3. Ataxia (2013) The mayo clinic. http://www.mayoclinic.com/health/ataxia/DS00910. Accessed 13 May 2013
4. Ataxias: General Classification (2013) Neuromuscular. neuromuscular.wustl.edu/ataxia/aindex.html. Accessed 13 May 2013
5. Bastian A, Martin T, Keating J, Thach W (1996) Cerebellar ataxia: abnormal control of interaction torques across multiple joints. J Neurophys 76:492–509
6. Bastian A, Zackowki K, Thach W (2000) Cerebellar ataxia: torque deficiency or torque mismatch between joints? J Neurophysiol 83(5):3019–3030
7. Brewer B, Fagan M, Klatzky R, Matsuoka Y (2005) Perceptual limits for a robotic rehabilitation environment using visual feedback distortion. Trans Neural Syst Rehabil Eng 13:1–11
8. Diedrichsen J, White O, Newman D, Lally N (2010) Use-dependent and error-based learning of motor behaviors. J Neurosci 30(15):5159–5166
9. Dolan J, Friedman M, Nagurka M (1993) Dynamic and loaded impedance components in the maintenance of human arm posture. IEEE Trans Syst Man Cybern Syst 23(3):698–709
10. Earhart G, Fletcher W, Horak F, Block E, Weber K, Suchowersky O, Melvill J (2002) Does the cerebellum play a role in podokinetic adaptation? Exp Brain Res 146(4):538–542
11. Emken J, Reinkensmeyer D (2005) Robot-enhanced motor learning: accelerating internal model formation during locomotion by transient dynamic amplification. Trans Neural Sys Rehabil Eng 13(1):33–39
12. Fasoli S, Fragala-Pinkham M, Hughes R, Hogan N, Krebs H, Stein J (2008) Upper limb robotic therapy for children with hemiplegia. Am J Phys Med Rehabil 87:929–936
13. Ghez C, Thach W (2000) The cerebellum. In: Kandel E, Schwartz J, Jessell J (eds) Principles of neural science. McGraw-Hill, New York
14. Gomi H, Kawato M (1997) Human arm stiffness and equilibrium-point trajectory during multi-joint movement. Biol Cybern 76(3):163–171
15. Grow D (2011) Robot-assisted modeling and rehabilitation strategies for cerebellar Ataxia. Dissertation, Johns Hopkins University
16. Hollerbach J, Khalil W, Gautier M (2008) Model identification. In: Sciliano B, Khatib O (eds) Springer handbook of robotics. Springer, New York, pp 321–342
17. Krebs H, Volpe B, Aisen M, Hogan N (2000) Increasing productivity and quality of care: robot-aided neuro-rehabilitation. J Rehabil Res Dev 37(6):639–652
18. Lum P, Burgar C, Shor P, Majmundar M, Van der Loos M (2002) Robot-assisted movement training compared with conventional therapy techniques for the rehabilitation of upper-limb motor function after stroke. Arch Phys Med Rehabil 83(7):952–959
19. Martin T, Keating J, Goodkin H, Bastian A, Thach W (1996) Throwing while looking through prisms: I. Focal olivocerebellar lesions impair adaptation. Brain 119:1183–1198
20. Maschke M, Gomez C, Ebner T, Konczak J (2004) Hereditary cerebellar ataxia progressively impairs force adaptation during goal-directed arm movements. J Neurophys 91(1):230–238
21. Massaquoi S, Hallett M (1996) Kinematics of initiating a two-joint arm movement in patients with cerebellar ataxia. Can J Neuro Sci 23(1):3–14
22. Miall R, Weir D, Wolpert D, Stein J (1993) Is the cerebellum a Smith predictor? J Motor Behav 25:203–216
23. Mobasser F, Hashtrudi-Zaad K (2006) A method for online estimation of human arm dynamics. Paper presented at the 28th EMBS, New York, 31 Aug–3 Sept 2006
24. Morton S, Bastian A (2006) Cerebellar contributions to locomotor adaptations during splitbelt treadmill walking. J Neurosci 26(36):9107–9116

25. Patton J, Stoykov M, Kovic M, Mussa-Ivaldi F (2006) Evaluation of robotic training forces that either enhance or reduce error in chronic hemiparetic stroke survivors. Exp Brain Res 168(3):368–383
26. Pigeon P, Bortolami S, DiZio P, Lackner J (2003) Coordinated turn-and-reach movements. I. Anticipatory compensation for self-generated coriolis and interaction torques. J Neurophys 89(1):276–289
27. Scheidt R, Stoeckmann T (2007) Reach adaptation and final position control amid environmental uncertainty after stroke. J Neurophys 97(4):2824–2836
28. Schweighofer N, Arbib M, Kawato M (1998) Role of the cerebellum in reaching movements in humans: I. Distributed inverse dynamics control. Eur J Neurosci 10(1):86–94
29. Scott S (1999) Apparatus for measuring and perturbing shoulder and elbow joint positions and torques during reaching. J Neurosci Methods 89:119–127
30. Smith E (2004) Robotic compensation of cerebellar ataxia. Thesis, Massachusetts Institute of Technology
31. Smith M, Shadmehr R (2005) Intact ability to learn internal models of arm dynamics in Huntington's disease but not cerebellar degeneration. J Neurophys 93(5):2809–2821
32. Stein J, Krebs H, Frontera W, Fasoli S, Hughes R, Hogan N (2004) Comparison of two techniques of robot-aided upper limb exercise training after stroke. Am J Phys Med Rehabil 83(9):720–728
33. Topka H, Konczak J, Schneider K, Boose A, Dichgans J (1998) Multi-joint arm movements in cerebellar ataxia: abnormal control of movement dynamics. Exp Brain Res 119(4):493–503
34. Trouillas P et al (1997) International cooperative ataxia rating scale for pharmacological assessment of the cerebellar syndrome. J Neuro Sci 145(2):205–211
35. Van der Loos H (1995) VA/Stanford rehabilitation robotics research and development program: lessons learned in the application of robotics technology to the field of rehabilitation. IEEE Trans Rehabil Eng 3(1):46–55
36. Westlake K, Patten C (2009) Pilot study of lokomat versus manual-assisted treadmill training for locomotor recovery post-stroke. J Neuroeng Rehabil 6(1):8–18